

Intensification of winter transatlantic aviation turbulence in response to climate change

Paul D. Williams^{1*} and Manoj M. Joshi²

Atmospheric turbulence causes most weather-related aircraft incidents¹. Commercial aircraft encounter moderate-or-greater turbulence tens of thousands of times each year worldwide, injuring probably hundreds of passengers (occasionally fatally), costing airlines tens of millions of dollars and causing structural damage to planes^{1–3}. Clear-air turbulence is especially difficult to avoid, because it cannot be seen by pilots or detected by satellites or on-board radar^{4,5}. Clear-air turbulence is linked to atmospheric jet streams^{6,7}, which are projected to be strengthened by anthropogenic climate change⁸. However, the response of clear-air turbulence to projected climate change has not previously been studied. Here we show using climate model simulations that clear-air turbulence changes significantly within the transatlantic flight corridor when the concentration of carbon dioxide in the atmosphere is doubled. At cruise altitudes within 50–75° N and 10–60° W in winter, most clear-air turbulence measures show a 10–40% increase in the median strength of turbulence and a 40–170% increase in the frequency of occurrence of moderate-or-greater turbulence. Our results suggest that climate change will lead to bumpier transatlantic flights by the middle of this century. Journey times may lengthen and fuel consumption and emissions may increase. Aviation is partly responsible for changing the climate⁹, but our findings show for the first time how climate change could affect aviation.

Aircraft experience turbulence when they encounter vertical airflow that varies on horizontal length scales greater than, but roughly equal to, the size of the plane¹. This equates to scales in the range 100 m–2 km for large, commercial aircraft¹⁰. Vertical airflow on these scales is associated with two distinct physical mechanisms: wave breaking caused by shear instabilities in clear air, and convective updraughts and downdraughts in and around clouds and thunder storms. Unlike convectively induced turbulence, clear-air turbulence cannot be avoided by using satellites and on-board radar to detect and circumvent clouds. For this reason, aircraft are estimated to spend about 3% of their cruise time in clear-air turbulence of at least light intensity¹¹, and about 1% of their cruise time in clear-air turbulence of at least moderate intensity¹. Despite recent advances¹⁰ and new observational techniques¹², the detailed mechanisms by which aviation turbulence is generated are still not fully understood. However, observational studies¹¹ suggest that clear-air turbulence is caused by Kelvin–Helmholtz instability, which generates turbulent billows when the destabilizing influence of vertical wind shear is sufficient to overcome the stabilizing influence of stratification. Gravity waves, including those launched by airflow over mountains, may play a crucial role in locally increasing the shear and initiating clear-air turbulence¹³.

The impacts of clear-air turbulence on aviation are reduced by the regular issuance of operational forecasts predicting when and where it will strike. At present, it is not computationally feasible to forecast turbulent eddies on horizontal scales of 100 m–2 km through explicit simulation with a global model of the troposphere and lower stratosphere. Instead, clear-air turbulence is forecast by computing various diagnostic measures derived from simulations of the larger-scale flow. Examples are the Colson–Panofsky index¹⁴, the Brown index¹⁵ and the Ellrod indices¹⁶. The instabilities diagnosed by these indices are necessary but not sufficient conditions for clear-air turbulence¹⁷. The second Graphical Turbulence Guidance (GTG2) algorithm, which is an optimally weighted linear combination of nine or ten diagnostics, validates well against pilot reports of turbulence¹. New diagnostics, inspired by laboratory observations of the generation of gravity waves^{18,19}, are still being developed and seem to hold promise for improving clear-air turbulence forecasts^{20,21}. Operationally, two World Area Forecast Centres (WAFC London and WAFC Washington) issue global forecasts of turbulence and other aviation hazards four times daily, under the supervision of the International Civil Aviation Organisation. The WAFC clear-air turbulence forecasts, which are produced by calculating variant 1 of Ellrod's turbulence index¹⁶, have shown significant skill when verified objectively against *in situ* observations from a fleet of British Airways aircraft²².

Here we enquire whether the incidence of clear-air turbulence might change in response to anthropogenic climate change. Although there have been suggestions of recent increases in aircraft bumpiness, the evidence has not been compelling. For example, four clear-air turbulence diagnostics have been found to increase by 40–90% over the period 1958–2001 in the North Atlantic, USA and European sectors in reanalysis data¹⁷. However, changes in the amount and type of assimilated data may partly account for these trends. In addition, moderate-or-greater upper-level turbulence has been found to increase over the period 1994–2005 in pilot reports in the United States²³. However, it is difficult to assign much significance to this trend, because of the shortness of the data set.

To investigate the response of clear-air turbulence to climate change, we use simulations from the Geophysical Fluid Dynamics Laboratory (GFDL) CM2.1 coupled atmosphere–ocean model^{24,25} (see Methods). We use 20 years of daily-mean data from two model integrations, each with prescribed concentrations of atmospheric CO₂. From the 500-year control integration, in which CO₂ is held constant at its pre-industrial value, we take daily data from years 161 to 180. From the 220-year climate-change integration, in which CO₂ increases at 1% per year for the first 70 years and then is held constant at twice its pre-industrial value, we take daily data from years 201 to 220. Note that CO₂ is projected to reach twice its

¹National Centre for Atmospheric Science, Department of Meteorology, University of Reading, Earley Gate, Reading RG6 6BB, UK, ²School of Environmental Sciences, University of East Anglia, Norwich Research Park, Norwich NR4 7TJ, UK. *e-mail: p.d.williams@reading.ac.uk

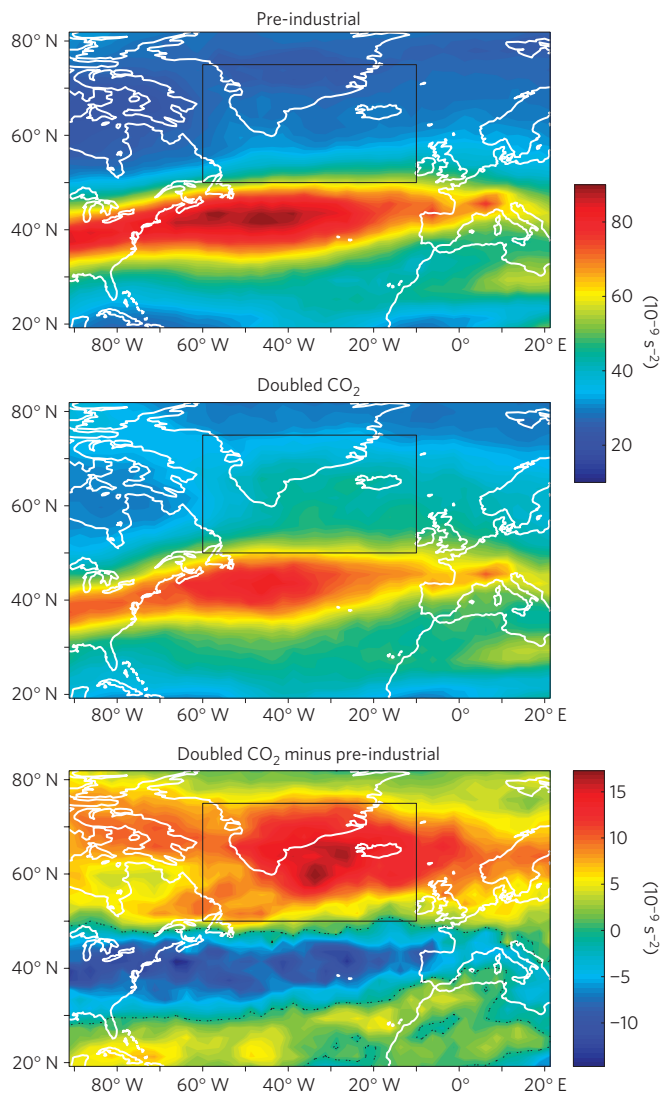


Figure 1 | Spatial patterns of North Atlantic flight-level winter clear-air turbulence in a changing climate. The quantity shown is the median of variant 1 of Ellrod's turbulence index, computed from 20 years of daily-mean data in December, January and February at 200 hPa. The top two panels are from pre-industrial and doubled-CO₂ integrations, and the bottom panel is the difference. The black dotted line in the bottom panel is the zero contour. The rectangles outline the area analysed in Fig. 2 and Table 1.

pre-industrial value by the middle of this century according to the commonly used A1B emissions scenario²⁶, which lies between the fossil-intensive and non-fossil scenarios. We focus on the months of December, January and February, which are when Northern Hemispheric clear-air turbulence is thought to be most intense¹⁷. We calculate clear-air turbulence diagnostics from the daily-mean temperature and wind fields at the 200 hPa pressure level, which is within the permitted cruise altitudes²⁷. We focus on the North Atlantic flight corridor between Europe and North America, which is the airspace within 30–75° N and 10–60° W. This flight corridor is one of the world's busiest, containing approximately 300 eastbound and 300 westbound flights per day²⁷.

We first calculate variant 1 of Ellrod's turbulence index¹⁶, which is defined to be the magnitude of the product of the flow deformation and the vertical wind shear. This empirical index is one of the most widely used clear-air turbulence diagnostics, showing significant skill when used for operational forecasts^{1,22}.

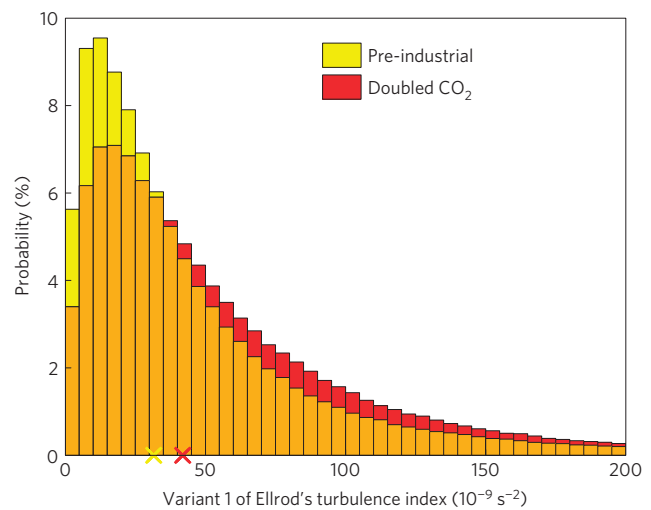


Figure 2 | Probability distributions of northern North Atlantic flight-level winter clear-air turbulence in a changing climate. The probabilities of lying within consecutive bins of width $5 \times 10^{-9} \text{ s}^{-2}$ are computed from 20 years of daily-mean data in December, January and February, at 200 hPa and within 50–75° N and 10–60° W. Two histograms are over-plotted, from the pre-industrial and doubled-CO₂ integrations. The overlap between the two distributions is shaded orange. The two crosses on the turbulence axis indicate the medians.

Maps of the spatial structure of the median are shown in Fig. 1. The index is non-negative by definition, and higher values indicate more turbulence. In both integrations, a band of relatively intense turbulence spans the width of the North Atlantic Ocean at about 40–50° N, coincident with the latitude of the jet stream. A similar structure is seen when turbulence diagnostics are calculated from reanalysis data¹⁷. In the doubled-CO₂ integration, the turbulence is considerably weaker in this band and stronger to the north, consistent with the poleward migration of the jet stream reported in this model²⁸. Maps of percentiles other than the 50th have similar spatial structures (not shown).

Probability distributions of the Ellrod index, in the northern half of the North Atlantic flight corridor, are shown as histograms in Fig. 2. The histograms in both integrations are uni-modal but non-Gaussian and positively skewed. Compared with the pre-industrial histogram, the doubled-CO₂ histogram is wider and less peaked, with probability density spread out to higher values. The longer tail indicates a shift towards stronger turbulence. The non-parametric two-sided Kolmogorov–Smirnov test clearly rejects the null hypothesis that the two histograms are different samples drawn from the same underlying distribution ($p \sim 10^{-5}$, $n = 554$). The test is performed after randomly under-sampling the spatio-temporal data by a factor of 1,000, because data separated by ten days, ten latitudinal grid points and ten longitudinal grid points are not significantly correlated. The medians of the two distributions are 31.5×10^{-9} and $41.9 \times 10^{-9} \text{ s}^{-2}$, corresponding to an increase of 32.8%. These medians are significantly different from each other, according to the non-parametric two-sided Mann–Whitney test, which is also performed after random under-sampling ($p \sim 10^{-6}$, $n = 554$).

Mindful that variant 1 of Ellrod's turbulence index is only one of many clear-air turbulence diagnostics to have been proposed, we next repeat the above calculations for 20 other diagnostics, each believed or demonstrated to have predictive skill¹. The 21 diagnostics are listed in Table 1. The list includes theoretical diagnostics related to shear instabilities (for example, the Richardson number), theoretical diagnostics indicating the emission of gravity waves (for example, the relative vorticity advection and the residual of

Table 1 | Northern North Atlantic flight-level winter clear-air turbulence in a changing climate.

Diagnostic	Units	Pre-industrial median	Doubled-CO ₂ median	Change (%) in median	Change (%) in frequency of MOG
Magnitude of potential vorticity	PVU	6.84	6.86	+0.3	+106.0
Colson–Panofsky index*	10 ³ kt ²	−34.8	−34.3	+1.5	+167.7
Brown index	10 ^{−6} s ^{−1}	77.1	79.2	+2.7	+95.5
Magnitude of horizontal temperature gradient*	10 ^{−6} K m ^{−1}	5.75	6.46	+12.2	+45.3
Magnitude of horizontal divergence	10 ^{−6} s ^{−1}	2.82	3.17	+12.3	+110.4
Magnitude of vertical shear of horizontal wind	10 ^{−3} s ^{−1}	1.88	2.14	+13.8	−1.0
Wind speed times directional shear	10 ^{−3} rad s ^{−1}	0.952	1.088	+14.2	+142.8
Flow deformation	10 ^{−6} s ^{−1}	18.6	21.5	+15.6	+96.0
Wind speed	m s ^{−1}	14.9	17.3	+16.3	+94.8
Flow deformation times vertical temperature gradient	10 ^{−9} K m ^{−1} s ^{−1}	8.17	9.97	+22.0	+147.3
Negative Richardson number*	−	−127.2	−97.9	+23.0	+3.2
Magnitude of relative vorticity advection	10 ^{−10} s ²	2.33	2.95	+26.7	+138.2
Magnitude of residual of nonlinear balance equation*	10 ^{−12} s ^{−2}	161	204	+27.1	+73.8
Negative absolute vorticity advection	10 ^{−10} s ^{−2}	2.05	2.63	+28.2	+144.0
Brown energy dissipation rate	10 ^{−6} J kg ^{−1} s ^{−1}	116	151	+30.0	+7.9
Relative vorticity squared	10 ^{−9} s ^{−2}	0.221	0.293	+32.5	+86.2
Variant 1 of Ellrod's turbulence index*	10 ^{−9} s ^{−2}	31.5	41.9	+32.8	+10.8
Flow deformation times wind speed	10 ^{−3} m s ^{−2}	0.251	0.341	+35.9	+92.9
Variant 2 of Ellrod's turbulence index	10 ^{−9} s ^{−2}	28.8	39.4	+36.8	+11.6
Frontogenesis function*	10 ^{−9} m ² s ^{−3} K ^{−2}	56.6	86.1	+52.1	+125.6
Version 1 of North Carolina State University index*	10 ^{−18} s ^{−3}	11.1	22.5	+102.9	+63.6

The table lists 21 clear-air turbulence diagnostics, together with their medians in the pre-industrial and doubled-CO₂ integrations and the percentage change. The table also lists the percentage change in the frequency of occurrence of moderate-or-greater (MOG) clear-air turbulence. The diagnostics have their usual definitions^{1,14–16,20} and are ranked according to the size of the percentage change in the median. Asterisks indicate GTG2 upper-level diagnostics¹. The statistics are computed from 20 years of daily-mean data in December, January and February, at 200 hPa and within 50–75° N and 10–60° W. If the pre-industrial median is negative, its absolute value has been used as the baseline to calculate the percentage change.

the nonlinear balance equation) and empirical diagnostics used by the airlines (for example, the negative absolute vorticity advection and the horizontal temperature gradient). The list includes seven of the ten GTG2 upper-level diagnostics¹; the remaining three are absent because they require numerical values for model-dependent fitting parameters, which are unknown for GFDL-CM2.1. Note that clear-air turbulence diagnostics were not designed to indicate mountain-wave turbulence, which is important particularly over Greenland, but this limitation does not compromise their ability to indicate other sources of clear-air turbulence over mountainous regions, such as sheared flow and loss of balance. For each of the 21 diagnostics, higher (more positive) values indicate more turbulence. The medians of each of the diagnostics, evaluated in the northern half of the North Atlantic flight corridor for the pre-industrial and doubled-CO₂ integrations, are shown in Table 1. Each of the 21 diagnostics shows an increased median in the doubled-CO₂ integration. For 16 of the diagnostics, the increase is between 10 and 40%. For one of the diagnostics, the increase is slightly over 100%. For each diagnostic, the same statistical tests applied above show that the probability distributions and medians are significantly different in the two integrations (Kolmogorov–Smirnov: $p \sim 10^{-7}$ – 10^{-2} , $n = 554$; Mann–Whitney: $p \sim 10^{-9}$ – 10^{-2} , $n = 554$).

Changes to the right-hand tails of the probability distributions are of great practical interest, because light, moderate, severe and extreme clear-air turbulence are successively less common and occur further into the tails. To quantify these changes, for each diagnostic we calculate the 99th percentile of the probability distribution for the pre-industrial experiment, and take it to be a threshold value. This threshold corresponds approximately to the onset of moderate turbulence¹, with the vertical acceleration of the aircraft exceeding 0.5g and unsecured objects on-board being dislodged¹⁰. We then compute how often this threshold is exceeded in the doubled-CO₂ experiment, compared with the pre-industrial

experiment. Note that each percentile contains 5,544 samples and is well populated. The results are shown in Table 1. Twenty of the 21 diagnostics show an increase in the frequency of occurrence of moderate-or-greater clear-air turbulence in the doubled-CO₂ integration. For 16 of the diagnostics, the increase is between 40 and 170%. Many of the increases cluster around 100%, which corresponds to a doubling of the frequency of occurrence.

A synthesis map indicating the level of agreement between the changes in the 21 diagnostics is shown in Fig. 3. Considering the region 50–80° N and 90° W–20° E, at least two thirds of the diagnostics show an increase in the median at almost all (97%) of the grid points, and every single one of the diagnostics shows an increase in the median at over one third (36%) of the grid points. Most or all of the British Isles, Norway, Sweden and Iceland lie within grid boxes at which 21 out of 21 diagnostics show an increase. Further south, a band in which the median is significantly increased stretches across the Atlantic Ocean from Central America to North Africa. At most grid points between 30° N and 50° N at these longitudes, there is no clear agreement on the sign of the change to the median, with roughly as many diagnostics showing a decrease as an increase.

In summary, we have found that a basket of clear-air turbulence measures diagnosed from climate simulations is significantly modified if the atmospheric CO₂ is doubled. In particular, at typical cruise altitudes in the northern half of the North Atlantic flight corridor in winter, most diagnostics show a 10–40% increase in the median strength of turbulence and a 40–170% increase in the frequency of occurrence of moderate-or-greater turbulence. To quantify the importance of the region of increased turbulence for aviation, we note that at present 61% of winter flight tracks within the North Atlantic flight corridor are north of 50° N, as estimated from a radar-based inventory of fuel burn (L. Wilcox, personal communication). We conclude that climate change will lead to bumpier transatlantic flights by the middle of this century,

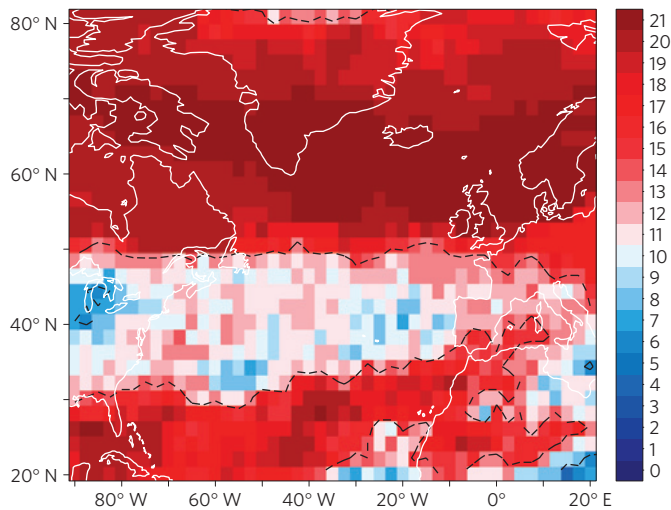


Figure 3 | Will North Atlantic flight-level winter clear-air turbulence increase or decrease in a warmer climate? The quantity shown is the number of the 21 clear-air turbulence diagnostics listed in Table 1 to show an increase in the median, in the doubled- CO_2 integration relative to the pre-industrial integration. The 21 medians are computed at each model grid point from 20 years of daily-mean data in December, January and February at 200 hPa. Red shading indicates that most of the diagnostics show an increase, and blue shading indicates that most show a decrease. The black dashed lines, which are contours at 7 and 14, delineate the regions in which at least two-thirds of the diagnostics agree on the sign of the change. Within these regions, the agreement on the sign of the change is significant at the 90% level, as assessed using the binomial distribution under the null hypothesis that each of the diagnostics is independent and equally likely to increase or decrease.

assuming the same flight tracks are used. Observational evidence suggests that this increase in bumpiness has already begun^{17,23}. Flight paths may need to become more convoluted to avoid patches of turbulence that are stronger and more frequent, in which case journey times will lengthen and fuel consumption and emissions will increase, in the same season and location that contrails have their largest climatic impact⁹. Finally, any increase in clear-air turbulence could have important implications for the large-scale atmospheric circulation, because clear-air turbulence contributes significantly to troposphere–stratosphere exchange¹⁷.

There are consequences of using finite-resolution daily-mean data to calculate turbulence diagnostics. For example, the threshold gradient Richardson number for instability leading to turbulence is 0.25 in continuous vertical coordinates, but is found empirically to be 20 with finite vertical resolution¹. We infer that turbulence diagnostics are generally functions of the spacetime sampling, and that they may be biased when calculated from gridded or averaged data. In addition, climate models may underestimate extreme events, so the 99th percentiles of the turbulence diagnostics may be biased. However, these biases affect the absolute values of the turbulence diagnostics, whereas our conclusions are based on the relative changes from the pre-industrial integration to the doubled- CO_2 integration, and are therefore expected to be robust.

As caveats, it is important to note that aviation turbulence is experienced by passengers and crew through quantities such as vertical acceleration, which are not necessarily linearly related to the turbulence diagnostics computed herein. Therefore, a given percentage increase in a turbulence diagnostic does not necessarily imply the same percentage increase in the sensation of turbulence by travellers. In addition, our study has not considered in-cloud turbulence or mountain-wave turbulence, which are important locally near storms and mountainous terrain,

and which may also be susceptible to climate change. Finally, GFDL-CM2.1 is only one climate model and A1B is only one future emissions scenario. Further work is needed to quantify the impacts of climate change on passenger-relevant measures of aviation turbulence from all sources, together with their model and scenario dependencies.

Methods

The GFDL-CM2.1 coupled atmosphere–ocean model^{24,25} is version 2.1 of the climate model from the GFDL. The model data are obtained from the World Climate Research Programme's (WCRP's) third Coupled Model Intercomparison Project (CMIP3) multi-model data set²⁹. The simulated atmosphere has a resolution of 2.5° in longitude and 2.0° in latitude, which is slightly coarser than the resolution used in other diagnostic studies¹⁷ because of the long integrations required here. The simulated atmosphere has 24 levels, of which five are above 200 hPa, approximately equivalent to an altitude of 12 km (39,000 ft) and close to typical cruise altitudes. The vertical resolution around the 200 hPa level is 50 hPa. This model is chosen because it has a high top level and data are available at daily resolution. The simulated upper-level winds in the northern extra-tropics agree well with two independently produced sets of reanalysis data^{24,30}, although the atmosphere at 200 hPa over ocean is particularly challenging to verify. The simulated upper-level jet stream in the North Atlantic sector strengthens and shifts towards the pole under global warming²⁸, consistent with the other CMIP3 models⁸. The simulated global warming in response to a doubling of the concentration of atmospheric CO_2 is near the median of the responses documented for the climate models used in the Intergovernmental Panel on Climate Change Third Assessment Report²⁸.

Received 12 November 2012; accepted 5 March 2013;
published online 8 April 2013

References

- Sharman, R., Tebaldi, C., Wiener, G. & Wolff, J. An integrated approach to mid- and upper-level turbulence forecasting. *Weather Forecast.* **21**, 268–287 (2006).
- Clark, T. L. *et al.* Origins of aircraft-damaging clear-air turbulence during the 9 December 1992 Colorado downslope windstorm: Numerical simulations and comparison with observations. *J. Atmos. Sci.* **57**, 1105–1131 (2000).
- Sharman, R. D., Trier, S. B., Lane, T. P. & Doyle, J. D. Sources and dynamics of turbulence in the upper troposphere and lower stratosphere: A review. *Geophys. Res. Lett.* **39**, L12803 (2012).
- Kennedy, P. J. & Shapiro, M. A. Further encounters with clear air turbulence in research aircraft. *J. Atmos. Sci.* **37**, 986–993 (1980).
- Knox, J. A. Possible mechanisms of clear-air turbulence in strongly anticyclonic flows. *Mon. Weath. Rev.* **125**, 1251–1259 (1997).
- Reiter, E. R. & Nania, A. Jet-stream structure and clear-air turbulence (CAT). *J. Appl. Meteorol.* **3**, 247–260 (1964).
- Koch, S. E. *et al.* Turbulence and gravity waves within an upper-level front. *J. Atmos. Sci.* **62**, 3885–3908 (2005).
- Lorenz, D. J. & DeWeaver, E. T. Tropopause height and zonal wind response to global warming in the IPCC scenario integrations. *J. Geophys. Res.* **112**, D10119 (2007).
- Stuber, N., Forster, P., Rädcl, G. & Shine, K. The importance of the diurnal and annual cycle of air traffic for contrail radiative forcing. *Nature* **441**, 864–867 (2006).
- Lane, T. P., Sharman, R. D., Trier, S. B., Fovell, R. G. & Williams, J. K. Recent advances in the understanding of near-cloud turbulence. *Bull. Am. Meteorol. Soc.* **93**, 499–515 (2012).
- Watkins, C. D. & Browning, K. A. The detection of clear air turbulence by radar. *Phys. Technol.* **4**, 28–61 (1973).
- Harrison, R. G., Heath, A. M., Hogan, R. J. & Rogers, G. W. Comparison of balloon-carried atmospheric motion sensors with Doppler lidar turbulence measurements. *Rev. Scient. Instr.* **80**, 026108 (2009).
- McCann, D. W. Gravity waves, unbalanced flow, and clear air turbulence. *Natl Weath. Digest.* **25**, 3–14 (2001).
- Colson, D. & Panofsky, H. A. An index of clear-air turbulence. *Q. J. R. Meteorol. Soc.* **91**, 507–513 (1965).
- Brown, R. New indices to locate clear-air turbulence. *Meteorol. Mag.* **102**, 347–360 (1973).
- Ellrod, G. P. & Knapp, D. L. An objective clear-air turbulence forecasting technique: Verification and operational use. *Weather Forecast.* **7**, 150–165 (1992).
- Jaeger, E. B. & Sprenger, M. A Northern Hemispheric climatology of indices for clear air turbulence in the tropopause region derived from ERA40 reanalysis data. *J. Geophys. Res.* **112**, D20106 (2007).
- Williams, P. D., Haine, T. W. N. & Read, P. L. On the generation mechanisms of short-scale unbalanced modes in rotating two-layer flows with vertical shear. *J. Fluid Mech.* **528**, 1–22 (2005).

19. Williams, P. D., Haine, T. W. N. & Read, P. L. Inertia–gravity waves emitted from balanced flow: Observations, properties, and consequences. *J. Atmos. Sci.* **65**, 3543–3556 (2008).
20. Knox, J. A., McCann, D. W. & Williams, P. D. Application of the Lighthill–Ford theory of spontaneous imbalance to clear-air turbulence forecasting. *J. Atmos. Sci.* **65**, 3292–3304 (2008).
21. McCann, D. W., Knox, J. A. & Williams, P. D. An improvement in clear-air turbulence forecasting based on spontaneous imbalance theory: the ULTURB algorithm. *Meteorol. Appl.* **19**, 71–78 (2012).
22. Gill, P. G. Objective verification of World Area Forecast Centre clear-air turbulence forecasts. *Meteorol. Appl.* <http://dx.doi.org/10.1002/met.1288> (2012).
23. Wolff, J. K. & Sharman, R. D. Climatology of upper-level turbulence over the contiguous United States. *J. Appl. Meteorol. Climatol.* **47**, 2198–2214 (2008).
24. Delworth, T. L. *et al.* GFDL’s CM2 global coupled climate models. Part I: Formulation and simulation characteristics. *J. Clim.* **19**, 643–674 (2006).
25. Gnanadesikan, A. *et al.* GFDL’s CM2 global coupled climate models. Part II: The baseline ocean simulation. *J. Clim.* **19**, 675–697 (2006).
26. Meehl, G. A. *et al.* in *IPCC Climate Change 2007: The Physical Science Basis* (eds Solomon, S. *et al.*) Ch. 10, 747–846 (Cambridge Univ. Press, 2007).
27. Irvine, E. A., Hoskins, B. J., Shine, K. P., Lunnon, R. W. & Froemming, C. Characterizing North Atlantic weather patterns for climate-optimal aircraft routing. *Meteorol. Appl.* **20**, 80–93 (2013).
28. Stouffer, R. J. *et al.* GFDL’s CM2 global coupled climate models. Part IV: Idealized climate response. *J. Clim.* **19**, 723–740 (2006).
29. Meehl, G. A. *et al.* The WCRP CMIP3 multi-model dataset: A new era in climate change research. *Bull. Am. Meteorol. Soc.* **88**, 1383–1394 (2007).
30. Reichler, T. & Kim, J. Uncertainties in the climate mean state of global observations, reanalyses, and the GFDL climate model. *J. Geophys. Res.* **113**, D05106 (2008).

Acknowledgements

P.D.W. is financially supported through a University Research Fellowship from the Royal Society (reference: UF080256). The authors acknowledge the modelling groups, the Program for Climate Model Diagnosis and Intercomparison (PCMDI) and the WCRP’s Working Group on Coupled Modelling (WGCM) for their roles in making available the WCRP CMIP3 multi-model data set. Support of this data set is provided by the Office of Science, US Department of Energy. The authors thank A. Turner for facilitating access to the data set. The authors thank E. Irvine and L. Wilcox for supplying information about flight routes, which were calculated using the Aviation Environmental Design Tool (AEDT) from the US Federal Aviation Administration (FAA).

Author contributions

P.D.W. and M.M.J. jointly conceived the study. P.D.W. computed the turbulence diagnostics, produced the figures and wrote the paper with input from M.M.J. The authors discussed the results and implications with each other at all stages.

Additional information

Reprints and permissions information is available online at www.nature.com/reprints. Correspondence and requests for materials should be addressed to P.D.W.

Competing financial interests

The authors declare no competing financial interests.